NASA/TM—2003-212353

ARL–TR–2970

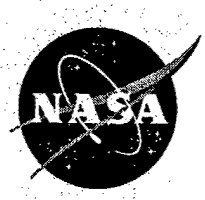

Evaluation of Low-Noise, Improved-Bearing-Contact Spiral Bevel Gears

David G. Lewicki
U.S. Army Research Laboratory, Glenn Research Center, Cleveland, Ohio

Ron L. Woods
Bell Helicopter Textron, Inc., Fort Worth, Texas

June 2003

The NASA STI Program Office . . . in Profile

Since its founding, NASA has been dedicated to the advancement of aeronautics and space science. The NASA Scientific and Technical Information (STI) Program Office plays a key part in helping NASA maintain this important role.

The NASA STI Program Office is operated by Langley Research Center, the Lead Center for NASA's scientific and technical information. The NASA STI Program Office provides access to the NASA STI Database, the largest collection of aeronautical and space science STI in the world. The Program Office is also NASA's institutional mechanism for disseminating the results of its research and development activities. These results are published by NASA in the NASA STI Report Series, which includes the following report types:

- TECHNICAL PUBLICATION. Reports of completed research or a major significant phase of research that present the results of NASA programs and include extensive data or theoretical analysis. Includes compilations of significant scientific and technical data and information deemed to be of continuing reference value. NASA's counterpart of peer-reviewed formal professional papers but has less stringent limitations on manuscript length and extent of graphic presentations.

- TECHNICAL MEMORANDUM. Scientific and technical findings that are preliminary or of specialized interest, e.g., quick release reports, working papers, and bibliographies that contain minimal annotation. Does not contain extensive analysis.

- CONTRACTOR REPORT. Scientific and technical findings by NASA-sponsored contractors and grantees.

- CONFERENCE PUBLICATION. Collected papers from scientific and technical conferences, symposia, seminars, or other meetings sponsored or cosponsored by NASA.

- SPECIAL PUBLICATION. Scientific, technical, or historical information from NASA programs, projects, and missions, often concerned with subjects having substantial public interest.

- TECHNICAL TRANSLATION. English-language translations of foreign scientific and technical material pertinent to NASA's mission.

Specialized services that complement the STI Program Office's diverse offerings include creating custom thesauri, building customized databases, organizing and publishing research results . . . even providing videos.

For more information about the NASA STI Program Office, see the following:

- Access the NASA STI Program Home Page at ***http://www.sti.nasa.gov***

- E-mail your question via the Internet to help@sti.nasa.gov

- Fax your question to the NASA Access Help Desk at 301–621–0134

- Telephone the NASA Access Help Desk at 301–621–0390

- Write to:
  NASA Access Help Desk
  NASA Center for AeroSpace Information
  7121 Standard Drive
  Hanover, MD 21076

NASA/TM—2003-212353

ARL–TR–2970

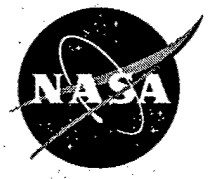

Evaluation of Low-Noise, Improved-Bearing-Contact Spiral Bevel Gears

David G. Lewicki
U.S. Army Research Laboratory, Glenn Research Center, Cleveland, Ohio

Ron L. Woods
Bell Helicopter Textron, Inc., Fort Worth, Texas

Prepared for the
59th Annual Forum and Technology Display
sponsored by the American Helicopter Society
Phoenix, Arizona, May 6–8, 2003

National Aeronautics and
Space Administration

Glenn Research Center

June 2003

The Propulsion and Power Program at
NASA Glenn Research Center sponsored this work.

Available from

NASA Center for Aerospace Information
7121 Standard Drive
Hanover, MD 21076

National Technical Information Service
5285 Port Royal Road
Springfield, VA 22100

Available electronically at http://gltrs.grc.nasa.gov

REPORT DOCUMENTATION PAGE

Form Approved
OMB No. 0704-0188

1. AGENCY USE ONLY (*Leave blank*)	2. REPORT DATE	3. REPORT TYPE AND DATES COVERED
	June 2003	Technical Memorandum

4. TITLE AND SUBTITLE

Evaluation of Low-Noise, Improved-Bearing-Contact Spiral Bevel Gears

5. FUNDING NUMBERS

WBS–22–708–90–01
1L162211A47A

6. AUTHOR(S)

David G. Lewicki and Ron L. Wood

7. PERFORMING ORGANIZATION NAME(S) AND ADDRESS(ES)

National Aeronautics and Space Administration
John H. Glenn Research Center at Lewis Field
Cleveland, Ohio 44135–3191

8. PERFORMING ORGANIZATION REPORT NUMBER

E–13941

9. SPONSORING/MONITORING AGENCY NAME(S) AND ADDRESS(ES)

National Aeronautics and Space Administration
Washington, DC 20546–0001
and
U.S. Army Research Laboratory
Adelphi, Maryland 20783–1145

10. SPONSORING/MONITORING AGENCY REPORT NUMBER

NASA TM—2003-212353
ARL–TR–2970

11. SUPPLEMENTARY NOTES

Prepared for the 59th Annual Forum and Technology Display sponsored by the American Helicopter Society, Phoenix, Arizona, May 6–8, 2003. David G. Lewicki, U.S. Army Research Laboratory, NASA Glenn Research Center; Ron L. Woods, Bell Helicopter Textron, Inc., Fort Worth, Texas 76101. Responsible person, David G. Lewicki, organization code 5950, 216–433–3970.

12a. DISTRIBUTION/AVAILABILITY STATEMENT

Unclassified - Unlimited
Subject Category: 37 Distribution: Nonstandard

Available electronically at http://gltrs.grc.nasa.gov

This publication is available from the NASA Center for AeroSpace Information, 301–621–0390.

12b. DISTRIBUTION CODE

13. ABSTRACT ***(Maximum 200 words)***

Studies to evaluate low-noise, improved-bearing-contact spiral-bevel gears were performed. Experimental tests were performed on the OH–58D helicopter main-rotor transmission in the NASA Glenn 500-hp Helicopter Transmission Test Stand. Low-noise, improved-bearing-contact spiral-bevel gears were compared to the baseline OH–58D spiral-bevel gear design, a high-strength design, and previously tested low-noise designs. Noise, vibration, and tooth strain tests were performed. The low-noise, improved-bearing-contact spiral-bevel design showed a decrease in noise compared to the baseline OH–58D design, but not as much reduction as previous tested low-noise designs. The low-noise, improved-bearing-contact spiral-bevel design gave the same benefit in reduced vibration compared to the baseline OH–58D design as that of the previously tested low-noise designs. The pinion tooth stresses for the low-noise, improved-bearing-contact spiral-bevel design showed a decrease compared to the baseline OH–58D design, but not quite as much as the previous tested high-strength and low-noise designs. For the low-noise, improved-bearing-contact design, the maximum stresses shifted toward the heel, compared to the center of the face width for the baseline, high-strength, and previously tested low-noise designs. Lastly, no hardline condition was found on the pinion tooth flank for the low-noise, improved-bearing-contact design.

14. SUBJECT TERMS

Strain gages; Vibration; Noise reduction; Spiral bevel gears; Bevel gears

15. NUMBER OF PAGES

28

16. PRICE CODE

17. SECURITY CLASSIFICATION OF REPORT	18. SECURITY CLASSIFICATION OF THIS PAGE	19. SECURITY CLASSIFICATION OF ABSTRACT	20. LIMITATION OF ABSTRACT
Unclassified	Unclassified	Unclassified	

Evaluation of Low-Noise, Improved-Bearing-Contact Spiral Bevel Gears

David G. Lewicki
U.S. Army Research Laboratory
National Aeronautics and Space Administration
Glenn Research Center
Cleveland, Ohio 44135

Ron L. Woods
Bell Helicopter Textron, Inc.
Fort Worth, Texas 76101

ABSTRACT—Studies to evaluate low-noise, improved-bearing-contact spiral-bevel gears were performed. Experimental tests were performed on the OH-58D helicopter main-rotor transmission in the NASA Glenn 500-hp Helicopter Transmission Test Stand. Low-noise, improved-bearing-contact spiral-bevel gears were compared to the baseline OH-58D spiral-bevel gear design, a high-strength design, and previously tested low-noise designs. Noise, vibration, and tooth strain tests were performed. The low-noise, improved-bearing-contact spiral-bevel design showed a decrease in noise compared to the baseline OH-58D design, but not as much reduction as previous tested low-noise designs. The low-noise, improved-bearing-contact spiral-bevel design gave the same benefit in reduced vibration compared to the baseline OH-58D design as that of the previously tested low-noise designs. The pinion tooth stresses for the low-noise, improved-bearing-contact spiral-bevel design showed a decrease compared to the baseline OH-58D design, but not quite as much as the previous tested high-strength and low-noise designs. For the low-noise, improved-bearing-contact design, the maximum stresses shifted toward the heel, compared to the center of the face width for the baseline, high-strength, and previously tested low-noise designs. Lastly, no hardline condition was found on the pinion tooth flank for the low-noise, improved-bearing-contact design.

INTRODUCTION

Spiral-bevel gears are used extensively in rotorcraft applications to transfer power and motion through non-parallel shafts. In helicopter applications, spiral-bevel gears are used in main-rotor and tail-rotor gearboxes to drive the rotors. In tilt-rotor applications, they are used in interconnecting drive systems to provide mechanical connection between two prop-rotors in case one engine becomes inoperable. Even though spiral-bevel gears have had considerable success in these applications, they are a main source of vibration in gearboxes, and thus, a main source of noise in cabin interiors [1-2]. In addition, higher strength and lower weight are required to meet the needs of future aircraft [3].

Various investigators have studied spiral-bevel gears and their influence on vibration and noise [4-6]. Most studies show that transmission error is directly related to undesirable vibration and noise. Transmission error is the difference of the actual rotation of the output gear minus the theoretical amount of rotation (equal to the rotation of the input pinion multiplied by the pinion to gear tooth ratio). A common practice is to modify spiral-bevel gear surface topology to permit operation in a misaligned mode to compensate for housing deflections. Over compensation for this type of operation, however, leads to large transmission error and higher noise and vibration levels.

In previous studies, gears with tooth fillet and root modifications to increase strength were manufactured and tested [7-8]. In addition, these previous studies tested gears with tooth surfaces designed for reduced transmission errors. The teeth were designed using the methods of Litvin and Zhang [9] to exhibit a parabolic function of transmission error at a controlled low level (8 to 10 arc sec). The low level of transmission error reduces the vibration and noise caused by the mesh. The new tooth geometries for this design were achieved through slight modification of the machine tool settings used in the manufacturing process. The design analyses addressed tooth generation, tooth contact analysis, transmission error prediction, and effects of misalignment [9-11]. The results from these tests showed a significant decrease in spiral-bevel gear noise, vibration, and tooth fillet stress. However, a hardline condition (concentrated wear lines) was present on the pinion tooth flank area. A hardline condition could possibly lead to premature failure such as early pitting/surface

fatigue, excessive wear, or scoring, and should be avoided in a proper gear design. Thus, subsequent analyses were performed to improve the gear tooth contact (eliminate the hard line) while maintaining low noise, vibration, and fillet stress [12]. These studies again used a pre-designed low level of parabolic transmission error constrained to have the bearing contact that avoids hardline conditions under design load.

The objective of this report is to describe the results of the experiments to evaluate the low-noise, improved-bearing-contact spiral-bevel gear design. Experimental tests were performed on the OH-58D helicopter main-rotor transmission in the NASA Glenn 500-hp Helicopter Transmission Test Stand. The low-noise, improved-bearing-contact spiral-bevel gear design was compared to the baseline OH-58D spiral-bevel gear design, a high-strength design, and the previous low-noise designs. Noise, vibration, and tooth strain test results are presented.

APPARATUS

OH–58D Main-Rotor Transmission

The OH–58 Kiowa is an Army single-engine, light, observation helicopter. The OH-58D is an advanced version developed under the Army Helicopter Improvement Program (AHIP). The OH–58D main-rotor transmission is shown in Fig. 1. It is currently rated at maximum continuous power of 410 kW (550 hp) at 6016 rpm input speed, with the capability of 10 sec torque transients to 475 kW (637 hp), occurring once per hour, maximum. The main-rotor transmission is a two-stage reduction gearbox with an overall reduction ratio of 15.23:1. The first stage is a spiral-bevel gear set with a 19-tooth pinion that meshes with a 62-tooth gear. Triplex ball bearings and one roller bearing support the bevel-pinion shaft. Duplex ball bearings and one roller bearing support the bevel-gear shaft. Both pinion and gear are straddle mounted.

A planetary mesh provides the second reduction stage. The bevel-gear shaft is splined to a sun gear shaft. The 27-tooth sun gear meshes with four 35-tooth planet gears, each supported with cylindrical roller bearings. The planet gears mesh with a 99-tooth fixed ring gear splined to the transmission housing. Power is taken out through the planet carrier splined to the output mast shaft. The output shaft is supported on top by a split-inner-race ball bearing and on the bottom by a roller bearing. The 62-tooth bevel gear also drives a 27-tooth accessory gear. The accessory gear runs an oil pump, which supplies lubrication through jets and passageways located in the transmission housing, as well as a hydraulic pump for aircraft controls.

Spiral-Bevel Test Gears

Four different spiral-bevel pinion and gear designs were compared. The first design was the baseline and used the current geometry of the OH-58D design. Table 1 lists basic design parameters. The reduction ratio of the bevel set is 3.26:1. All gears were made using standard aerospace practices where the surfaces were carburized and ground. The material used for all test gears was X-53 (AMS 6308). Two sets of the baseline design were tested.

The second spiral-bevel design was an increased strength design. The configuration was identical to the baseline except that the tooth fillet radius of the pinion was increased by a factor of approximately two. Also, the tooth fillet radius of the gear was slightly increased (approximately 1.16 times the baseline) and made full fillet. Tooth fillet radii larger than those on conventional gears were made possible by advances in spiral-bevel gear grinding technology. Advanced gear grinding was achieved through redesign of a current gear grinder and the addition of computer numerical control [13]. Two sets of the increased-strength design were tested.

The third spiral-bevel design was a previous low-noise design. The low-noise design was identical to the increased-strength design except the pinion teeth were slightly altered to reduce transmission error. The gear member was the same as in the increased-strength design. The low-noise design was based on the idea of local synthesis that provided at the mean contact point the following conditions of meshing and contact [4]: a) the required gear ratio and its derivative, b) the desired direction of the tangent to the contact path, and c) the desired orientation and size of the major axis of the instantaneous contact ellipse. The local synthesis was complemented with a tooth contact analysis [4]. Using this approach, the machine tool settings for reduced noise were determined. As with the high-strength design, precise control of the manufactured tooth surfaces was made possible by advances in the final grinding operation machine tool [13]. Further information on the previous low-noise design can be found in references [7-8]. In summary, the effect of the topological change in the low-noise design was a reduction in overall crowning of the tooth, leading to an increase in contact ratio and reduced transmission error.

Two sets of a first attempt of a low-noise design were tested. This included two low-noise pinions and two

gear members where the gear members were the same as the increased-strength design. In addition, one low-noise pinion with 0.050" TOPREM, one low-noise pinion with 0.090" TOPREM, and one low-noise pinion with 0.120" TOPREM, were tested. TOPREM is the decrease in the pressure angle at the tip of the grinding wheel used on the pinion during final machining. This decrease in pressure angle causes more stock to be removed in flank portion of the tooth to prevent interference with the top of the gear member during operation. The 0.050, 0.090, and 0.120" designations refer to the depth of modification along the blade cutting edge.

Lastly, the fourth spiral-bevel design was a new low-noise, improved-bearing-contact design. This new design was in general based on the principles of the previous low-noise design, but included an improved iterative approach balancing low transmission errors for reduced noise and tooth contact analysis to avoid adverse contact and concentrated wear conditions [12]. In addition, modified roll was used in the pinion generation, and finite element analysis was used to evaluate stress and contact conditions. One low-noise, improved-bearing-contact design pinion was tested.

NASA Glenn 500-HP Helicopter Transmission Test Stand

The OH-58D transmission was tested in the NASA Glenn 500-hp helicopter transmission test stand (Fig. 2). The test stand operates on the closed-loop or torque-regenerative principle. Mechanical power recirculates through a closed loop of gears and shafting, part of which is the test transmission. The output of the test transmission attaches to the bevel gearbox. The output shaft of the bevel gearbox passes through a hollow shaft in the closing-end gearbox and connects to the differential gearbox. The output of the differential attaches to the hollow shaft in the closing-end gearbox. The output of the closing-end gearbox connects to the speed increaser gearbox. The output of the speed increaser gearbox attaches to the input of the test transmission, thereby closing the loop.

A 149-kW (200-hp) variable-speed direct-current (d.c.) motor powers the test stand and controls the speed. The motor output attaches to the closing-end gearbox. The motor replenishes losses due to friction in the loop. An 11-kW (15-hp) d.c. motor provides the torque in the closed loop. This motor drives a magnetic particle clutch. The clutch output does not turn but exerts a torque. This torque is transferred through a speed reducer gearbox and a chain drive to a large sprocket on the differential gearbox. The torque on the sprocket applies torque in the closed loop by displacing the gear attached to the output shaft of the bevel gearbox with respect to the gear connected to the input shaft of the closing-end gearbox. This is done within the differential gearbox through use of a compound planetary system where the planet carrier attaches to the sprocket housing. The magnitude of torque in the loop is adjusted by changing the electric field strength of the magnetic particle clutch.

A mast shaft loading system in the test stand simulates rotor loads imposed on the OH-58D transmission output mast shaft. The OH-58D transmission output mast shaft connects to a loading yoke. Two vertical load cylinders connected to the yoke produce lift loads. A 14,000-kPa (2000-psig) nitrogen gas system powers the cylinders. Pressure regulators connected to the nitrogen supply of each of the load cylinders adjust the magnitude of lift. Note that in the OH-58D design, the transmission at no-load is misaligned with respect to the input shaft. At 18,309 N (4116 lb) mast lift load, the elastomeric corner mounts of the OH-58D transmission housing deflect such that the transmission is properly aligned with the input shaft (In the actual helicopter, this design serves to isolate the airframe from the rotor vibration).

The test transmission input and output shafts have speed sensors, torquemeters, and slip rings. Both load cylinders on the mast yoke are mounted to load cells. The 149-kW (200-hp) motor has a speed sensor and a torquemeter. The magnetic particle clutch has speed sensors on the input and output shafts and thermocouples. An external oil-water heat exchanger cools the test transmission oil. A facility oil-pumping and cooling system lubricates the differential, closing-end, speed increaser, and bevel gearboxes. The facility gearboxes have accelerometers, thermocouples, and chip detectors for health and condition monitoring.

TEST PROCEDURE

From the previous studies, two sets of the baseline design (a set consisted of a pinion and a gear), two sets of the high-strength design, and two sets of the previous low-noise design were manufactured and tested. Note that the gear members for the high-strength set and previous low-noise set were the same design. There were, however, four of these gear members manufactured, two for the high-strength set and two for the low-noise set. Again, these gears differed from the gear member of the baseline set (two if these manufactured and tested) due to the increased fillet radius and full fillet. Also from the previous studies, three additional low-noise design pinions with TOPREM modifications were manufactured and tested. These pinions meshed with one of the gear members of the previous low-noise set for all of their tests. For the current study, one low-noise,

improved-bearing-contact design pinion was manufactured and tested. This pinion meshed with one of the gear members of the high-strength set for all of its tests.

Noise and vibration tests were performed on all pinions and gears manufactured. One set of the baseline design, one set of the high-strength design, one set of the previous low-noise design, and the low-noise, improved-bearing-contact design pinion were all instrumented with strain gages and strain tests were performed on these. Again, the low-noise, improved-bearing-contact design pinion meshed with the instrumented gear member of the high-strength set for its strain tests. A description of the instrumentation, test procedure, and data reduction procedure is as follows.

Noise Tests

Acoustic intensity measurements were performed using the two-microphone technique. The microphones used had a flat response (±2 dB) up to 5000 Hz and a nominal sensitivity of 50 mV/Pa. The microphones were connected to a spectrum analyzer which computed the acoustic intensity from the imaginary part of the cross-power spectrum. Near the input region of the OH–58D transmission, a grid was installed which divided the region into 16 areas (Fig. 3). For each test, the acoustic intensity was measured at the center of each of the 16 areas. Only positive acoustic intensities (noise flowing out of the areas) were considered. The acoustic intensities were then added together and multiplied by the total area of the grids to obtain sound power of the transmission input region.

At the start of each test, the test transmission oil was heated using an external heater and pumping system. For all the tests, the oil used conformed to a DOD–L–85734 specification. Once the oil was heated, the transmission input speed was increased to 3000 rpm, a nominal amount of torque was applied, and mast lift load was applied to align the input shaft (18 310 N, 4120 lb). The transmission input speed and torque were then increased to the desired conditions. The tests were performed at 100-percent transmission input speed (6016 rpm) and torques of 50, 75, 100, and 125-percent of maximum design. The transmission oil inlet temperature was set at 99 °C (210 °F). After the transmission oil outlet stabilized (which usually required about 20 min), the acoustic intensity measurements were taken. The time to obtain the acoustic intensity measurements of the 16 grid points at a given test condition was about 30 min. For each acoustic intensity spectrum at a grid point, 100 frequency-domain averages were taken. This data was collected by a computer. The computer also computed the sound power spectrum of the grids after all the measurements were taken.

Vibration Tests

Eight piezoelectric accelerometers were mounted at various locations on the OH–58D transmission housing (Fig. 4). The accelerometers were located near the input spiral-bevel area (accelerometers 1and 2, measuring radially to the input shaft), the ring gear area (accelerometers 3 and 4, measuring radially to the planetary), and on the top cover (accelerometers 5 to 8, measuring vertically). All accelerometers had a 1 to 25 000-Hz (±3 dB) response, 4 mV/g sensitivity, and integral electronics. Fig. 5 shows a photograph of the noise and vibration test setup.

The vibration tests were performed in conjunction with the noise tests. After collecting the acoustic intensity data for a given test, the vibration data were recorded on tape and processed off-line. The vibration data were later analyzed using time averaging. Here, the vibration data recorded on tape were input to a signal analyzer along with a tach pulse from the transmission input shaft. The signal analyzer was triggered from the tach pulse to read the vibration data when the transmission input shaft was at the same position. The vibration signal was then averaged in the time domain using 100 averages. This technique removed all the vibration which was not synchronous to the input shaft. Before averaging, the major tones in the vibration spectrum of the OH–58D baseline design were the spiral-bevel and planetary gear fundamental frequencies and harmonics. Time averaging removed the planetary contribution, leaving the spiral-bevel contribution for comparing the different design configurations.

Strain Tests

Twenty strain gages were mounted on the spiral-bevel pinions for one set of each of the four designs (Fig. 6). Twenty-six gages were mounted on the spiral-bevel gears (Fig. 7). Gages were positioned across the tooth face widths with some in the fillet area and some in the root area of the teeth. The fillet gages were placed on the drive side of two adjacent teeth. The fillet gages were also positioned at a point on the tooth cross-section where a line at a 45° angle with respect to the tooth centerline intersects the tooth profile. The fillet gages were placed there to measure maximum tooth bending stress. (Previous studies on spur gears showed that the maximum stresses were at a line 30° to the tooth centerline [14]. Forty-five degrees was chosen for the current tests to minimize the possibility of the gages being destroyed due to tooth contact.) In addition to maximum tensile stresses, root stresses can become significant in lightweight, thin-rimmed aerospace gear applications [15]. Thus, root gages were centered between teeth in the root to measure gear rim stress.

Tooth fillet and root gages were placed on successive teeth to determine loading consistency. The grid length of the gages was 0.381 mm (0.015 in.) and the nominal resistance was 120 Ω. The gages were connected to conditioners using a Wheatstone bridge circuitry and using a quarter-bridge arrangement.

Static strain tests were performed on both the spiral-bevel pinions and gears. A crank was installed on the transmission input shaft to manually rotate the shaft to the desired position. A sensor was installed on the transmission output shaft to measure shaft position. At the start of a test, the transmission was completely unloaded and the strain gage conditioners were zeroed. Conditioner spans were then determined using shunt calibrations. The transmission was loaded (using the facility closed-loop system) to the desired torque, the shaft was positioned, and the strain readings along with shaft positions were obtained using a computer. This was done for a variety of positions to get strain as a function of shaft position for the different gages. At the end of a test, the transmission was again completely unloaded and the conditioner zeroes were checked for drift. A photograph of the static strain setup is shown in Fig. 8.

Dynamic strain tests were performed only on the spiral-bevel pinions. The pinion gages were connected to slip rings mounted on the input shaft. A slip ring assembly for the spiral-bevel gear was unavailable, and thus, dynamic strain tests of the gear were not performed. The test procedure was basically the same as the noise and vibration tests, except that the transmission was not run as long in order to maximize strain gage life. A photograph of the dynamic strain setup is shown in Fig. 9. The dynamic strain data were recorded on tape and processed off-line. The dynamic strain data were later digitized into a computer and time-averaged in a manner similar to the vibration data. This procedure was used to remove random slip ring noise.

RESULTS AND DISCUSSION

Noise Tests

Fig. 10 gives sound power as a function of torque. The depicted sound power is the sum of the sound power at the spiral-bevel meshing frequency (1905 Hz) and its first harmonic (3810 Hz). In inspecting the frequency content of the data, the sound power at the meshing frequency was dominant. As interpreted from the figure, the data is divided into three groups. The first group is the circles and squares, which are the baseline and increased strength designs. The sound power (i.e., noise from the bevel gear mesh) for these designs show a slight increase with torque. They give about the same trend with approximately 5 dB of scatter. This is expected since the bevel pinion and gear tooth geometries for this group were identical except for the fillet region.

The second group is the triangles, which are the original low-noise designs, with and without TOPREM. These data show a significant decrease in noise, especially at the 100% torque condition (about 16 dB). They give about the same trend with approximately 2 to 8 dB of scatter. The third group is the solid diamonds, which are the data from the low-noise, improved-bearing-contact design. The sound power from this design is nearly constant with torque. It shows a decrease in noise from the baseline design (about 7dB at 100% torque), but not as much reduction as the previous low-noise designs.

Vibration Tests

Fig. 11 gives the results from the vibration tests. Shown is acceleration as a function of torque for the eight accelerometers mounted on the OH-58 transmission housing. Again, the acceleration was time-averaged with respect to the input shaft to remove all non-synchronous vibration. In inspecting the frequency content of the data, the majority of the time-averaged vibration was from the spiral-bevel mesh. The data points in the figure are the root-mean-square (rms) values of the time-averaged vibration time traces. In general, each figure can be divided in two groups: 1) baseline and high-strength designs (circles and squares), and 2) low noise designs (triangles and diamonds). As with the noise results, there was a significant reduction in vibration for the low-noise designs compared to the baseline. For accelerometers 1, 3, 4, 5, 6, and 8, the vibration for all the low-noise designs are basically lumped together with a scatter of about 3 g's. The low-noise, improved-bearing-contact design gave the same benefit in reduced vibration as that of the previously tested low-noise designs. As with the noise test results, the vibration for the low-noise, improved-bearing-contact design was pretty much constant with torque. Note that cases where data are missing from the figure (low-noise, improved-bearing-contact pinion design for accelerometer #5, Fig. 11e, as an example) were due to faulty instrumentation.

Strain Tests

Set #2 (pinion and gear) of the baseline design, set #2 of the high-strength design, set #2 of the original low-noise design, and the low-noise, improved-bearing-contact pinion were instrumented with strain gages. The low-noise, improved-bearing-contact pinion meshed with the gear member of the high-strength design. Results of the

strain measurements will be presented both as plots of stresses as functions of shaft positions and tables of values summarizing the peak values.

First, results of the static strain tests at 100% torque for the pinion fillet gages are shown in Fig. 12. Shown is stress versus pinion shaft position for all the pinion fillet gages of the baseline, high-strength, original low-noise, and low-noise, improved-bearing-contact designs. Since the strain in the tooth fillet is mostly uniaxial and in the tangential direction of the tooth face [16], the stress was calculated by multiplying the measured strain by the modulus of elasticity (30×10^6 psi for steel). The figure depicts results from fillet gages on adjacent gear teeth (gages 4 and 11, 5 and 12, 6 and 13, ...) for the seven positions along the gear tooth face width. Gages 4 and 11 correspond to positions at the heel of the pinion and gages 10 and 17 correspond to positions at the toe of the pinion. The gages show typical results of a driving pinion member rolling through mesh. As a driving pinion rolls through mesh, it first sees a small amount of compression in the fillet when the tooth ahead of the strain-gaged tooth is in contact with the driven gear. As the pinion rolls further through mesh, the strain-gaged tooth is in contact with the driver and the fillet region sees tensile stress. At the maximum stress, the strain-gaged tooth is loaded in single tooth contact. Note that cases where data are missing from the figure (baseline design gages 4, 5, 8, 9, and 10, as examples) were due to faulty gages.

For the pinion fillet gages at 100% torque, the maximum tensile stress occurred at the middle of the tooth face width for the baseline and high-strength designs (gage 6, 7, 13, and 14 regions; it should be noted that gages 6-8 and 13-15 were located as close to each other, respectively, as possible). The minimum stress (maximum compression) occurred slightly to the heel side of the middle of the tooth face width. The maximum alternating stress occurred at the same location of the maximum tensile stress, where the alternating stress is defined as the maximum stress minus the minimum stress for a given gage position. For the previously tested low-noise design, maximum values of the stresses (tensile, compressive, alternating) shifted slightly toward the toe compared to the baseline design. For the low-noise, improved-bearing-contact design, maximum values of the stresses (tensile, compressive, alternating) shifted significantly toward the heel compared to the baseline design. Table II lists the values of the maximum, minimum, and alternating stresses of the various designs tested at 100% torque. It should be noted that the values listed in the table were the average of the two row of the corresponding gages. In all cases the Change column compares the stress to the baseline design. From Table IIa, there was a significant reduction in pinion fillet maximum tensile stress of the high-strength design compared to the baseline. There was an even greater reduction for the original low-noise design. There was less of a reduction for the low-noise, improved-bearing-contact design, but it was still significant. There was a reduction in the absolute value of the minimum (compressive) stress for the low-noise, improved-bearing-contact design compared to the baseline, which led to a significant reduction in alternating stress compared to the baseline.

Figure 13 gives the results of the static strain tests at 100% torque for the gear fillet gages. The shapes of the stress-position traces look similar to that of the pinion except the fillet compression occurs after the tension. This is because the tooth ahead of the strain-gage tooth sees contact with the driver member after the strain-gaged tooth is in contact. For the baseline design, high-strength design, and original low-noise design, the maximum tensile stresses occurred at the middle of the tooth face width. For the low-noise, improved-bearing-contact design, the maximum tensile stress shifted toward the heel. From Table IIb, there was a significant reduction in gear fillet maximum tensile stress for the high-strength, low-noise, and low-noise, improved-bearing-contact designs compared to the baseline. The greatest benefit was from the low-noise, improved-bearing-contact design. Also, note that the magnitude of gear fillet tensile stresses was significantly lower than that of pinion. Lastly, cases where data are missing from the figure (low-noise, improved-bearing-contact pinion design gages 9 and 16) were due to faulty gages.

Figure 14 gives the results of the static strain tests at 100% torque for the pinion root gages. Although the root gages were physically located three teeth apart (Fig. 6), they are plotted as if they were on adjacent teeth. The stress-position traces were different than the fillet gages in that the maximum compression was nearly twice as great as the maximum tension. However, the magnitude of the maximum tension is significantly less than that in the fillet. As with the fillet gages, the maximum stresses (tensile and alternating) occurred at the middle of the tooth face width for the baseline design, high-strength design, and original low-noise design, and shifted toward to heel for the low-noise, improved-bearing-contact design. The same trend was observed for the gear root gages (Fig. 15). The maximum tensile stress in the pinion root significantly increased for the high-strength design, and original low-noise design compared to the baseline (Table IIc). The maximum tensile stress in the pinion root drastically increased for the low-noise, improved-bearing-contact design compared to the baseline. The alternating stresses in the pinion root of the high-strength, original low-noise, and low-noise, improved-bearing-contact

designs increased about the same amount compared to the baseline. The maximum tensile stress in the gear root significantly increased for the high-strength design compared to the baseline, but stayed the same for the original low-noise design and low-noise, improved-bearing-contact design (Table IId).

Figure 16 compares the dynamic and static stresses for the pinion fillet gages at 100% torque for the low-noise, improved-bearing-contact design. For the three gages shown (gages 12, 14, and 16), there was no apparent change in stresses due to dynamic effects. There was no change in shape of the stress-position traces and the maximum and minimum values were similar. This was typical for all the fillet gages (Table IIIa and IIIb). The same observation were found for the pinion root gages (Fig. 17, Tables IIIc and IIId).

Bevel Tooth Contact Patterns

As previously reported, the original low-noise designs showed a significant decrease in spiral-bevel gear noise, vibration, and tooth fillet stress [7-8]. However, a hard-line condition (concentrated wear lines) was present on the pinion tooth flank area for these designs. Figures 18 and 19 show close-up photographs of the pinion and gear, respectively, for the low-noise, improved-bearing-contact design after completion of all tests. No hardline condition was found on the pinion tooth flank.

SUMMARY OF RESULTS

Studies to evaluate low-noise, improved-bearing-contact spiral-bevel gears were performed. Experimental tests were performed on the OH-58D helicopter main-rotor transmission in the NASA Glenn 500-hp Helicopter Transmission Test Stand. Low-noise, improved-bearing-contact spiral-bevel gears were compared to the baseline OH-58D spiral-bevel gear design, a high-strength design, and previously tested low-noise designs. Noise, vibration, and tooth strain tests were performed. The following results were obtained:

1) The low-noise, improved-bearing-contact spiral-bevel design showed a decrease in noise compared to the baseline OH-58D design (about 7 dB at 100% torque), but not as much reduction as previous tested low-noise designs design (about 16 dB at 100% torque). The bevel mesh sound power for the low-noise, improved-bearing-contact spiral-bevel design was nearly constant with torque.

2) The low-noise, improved-bearing-contact spiral-bevel design gave the same benefit in reduced vibration compared to the baseline OH-58D design as that of the previously tested low-noise designs. As with the noise test results, the vibration for the low-noise, improved-bearing-contact design was nearly constant with torque.

3) The spiral-bevel pinion tooth stresses for the low-noise, improved-bearing-contact spiral-bevel design showed a significant decrease compared to the baseline OH-58D design, but not quite as much as the previous tested high-strength and low-noise designs. The gear stresses, however, showed a significant decrease compared to the baseline OH-58D design, even more than the previous tested high-strength and low-noise designs. For the low-noise, improved-bearing-contact design, the maximum stresses shifted toward the heel, compared to the center of the face width for the baseline, high-strength, and previously tested low-noise designs. There was no apparent change in stresses due to dynamic effects for the low-noise, improved-bearing-contact design.

4) No hardline condition was found on the pinion tooth flank for the low-noise, improved-bearing-contact design.

REFERENCES

1. Lewicki, D.G., and Coy, J.J., Vibration Characteristics of OH-58A Helicopter Main Rotor Transmission, 1987, NASA TP–2705, AVSCOM TR–86–C-42.
2. Mitchell, A.M., Oswald, F.B., and Coe, H.H., Testing of UH-60A Helicopter Transmission in NASA-Lewis 2240-kW (3000-hp) Facility, 1986, NASA TP–2626.
3. Vialle, M., "Tiger MGB-, High Reliability-, Low Weight," Proceedings of the 47th American Helicopter Society Annual Forum Proceedings, Vol. 2, AHS, Alexandria, VA, 1991, pp. 1249–1258.
4. Litvin, F.L., and Zhang, Y., Local Synthesis and Tooth Contact Analysis of Face-Milled Spiral Bevel Gears, 1991, NASA CR–4342, AVSCOM TR–90–C–28.
5. Gosselin, C., Cloutier, L., and Brousseau, J., Tooth Contact Analysis of High Conformity Spiral Bevel Gears, Proceedings of the International Conference on Motion and Power Transmissions, 1991, pp. 725–730.
6. Fong, Z.H., and Tsay, C.B., Kinematic Optimization of Spiral Bevel Gears, Journal of Mechanical Design, 1992, Vol. 114, No. 3, pp. 498–506.
7. Lewicki, D.G., Handschuh, R.F., Henry, Z.S., and Litvin, F.L., "Improvements in Spiral-Bevel Gears to Reduce Noise and Increase Strength," Proceedings of the 1994 International Gearing Conference, Sep. 1994, pp. 341–346.

8. Lewicki, D.G., Handschuh, R.F., Henry, Z.S., and Litvin, F.L., "Low-Noise, High-Strength, Spiral-Bevel Gears for Helicopter Transmissions," AIAA Journal of Propulsion and Power, Vol. 10, No. 3, May–Jun. 1994, pp. 356–361.
9. Litvin, F.L., and Zhang, Y., "Local Synthesis and Tooth Contact Analysis of Face-Milled Spiral Bevel Gears," NASA CR–4342, 1991.
10. Litvin, F.L., Zhang, Y., and Chen, J., "User's Manual for Tooth Contact Analysis of Face-Milled Spiral Bevel Gears With Given Machine-Tool Settings," NASA CR–189093, 1991.
11. Litvin, F.L., Kuan, C., and Zhang, Y., "Determination of Real Machine-Tool Settings and Minimization of Real Surface Deviation by Computer Inspection," NASA CR–4383, 1991.
12. Fuentes, A., Litvin, F.L., Mullins, B.R., Woods, R., Handschuh, R.F., and Lewicki, D.G., "Design and Stress Analysis of Low-Noise Adjusted-Bearing-Contact Spiral Bevel Gears," Proceedings of the International Conference on Gears, Munich, Germany, Vol. 1, Mar. 2002, pp. 327–340.
13. Scott, H.W., Computer Numerical Control Grinding of Spiral Bevel Gears, 1991, NASA CR–187175, AVSCOM TR–90–F–6.
14. Hirt, M.C.O., Stress in Spur Gear Teeth and Their Strength as Influenced by Fillet Radius, Ph.D. Dissertation, Technische Universitat Munchen, 1976, translated by the American Gear Manufacturers Association.
15. Drago, R.J., Design Guidelines for High-Capacity Bevel Gear Systems, AE-15 Gear Design, Manufacturing and Inspection Manual, Society of Automotive Engineers, 1990, pp. 105–121.
16. Winter, H., and Paul, M., Influence of Relative Displacements Between Pinion and Gear on Tooth Root Stresses of Spiral Bevel Gears, 1985, Journal of Mechanisms Transmissions and Automation in Design, Vol. 107, pp. 43–48.

Table I. Baseline spiral-bevel gear parameters of the OH-58D main-rotor transmission.

Number of teeth,	
pinion	19
gear	62
Module, mm (diametral pitch, in^{-1})	4.169 (6.092)
Pressure angle, deg	20
Mean spiral angle, deg	35
Shaft angle, deg	95
Face width, mm (in.)	36.83 (1.450)

Table II. Comparison of low-noise, improved-bearing-contact design static strain test results to previously tested results, 100% torque.

a) Pinion fillet gages.	Max Stress (ksi)	Change (%)	Min Stress (ksi)	Change (%)	Alt Stress (ksi)	Change (%)
Baseline design	126		-38		157	
High-strength design	92	-27.2%	-46	22.3%	136	-13.3%
Low-noise design	89	-29.4%	-35	-6.1%	114	-27.6%
Low-noise, improved-bearing-contact design	96	-24.4%	-26	-30.6%	116	-25.9%

b) Gear fillet gages.	Max Stress (ksi)	Change (%)	Min Stress (ksi)	Change (%)	Alt Stress (ksi)	Change (%)
Baseline design	88		-35		118	
High-strength design	77	-12.4%	-29	-15.1%	101	-14.4%
Low-noise design	71	-19.0%	-21	-38.4%	87	-26.3%
Low-noise, improved-bearing-contact design	56	-36.0%	-29	-16.5%	82	-30.4%

c) Pinion root gages.	Max Stress (ksi)	Change (%)	Min Stress (ksi)	Change (%)	Alt Stress (ksi)	Change (%)
Baseline design	33		-40		72	
High-strength design	41	24.7%	-76	91.2%	110	52.3%
Low-noise design	41	24.2%	-71	77.5%	110	51.3%
Low-noise, improved-bearing-contact design	57	74.2%	-54	35.9%	111	52.7%

d) Gear root gages.	Max Stress (ksi)	Change (%)	Min Stress (ksi)	Change (%)	Alt Stress (ksi)	Change (%)
Baseline design	30		-67		92	
High-strength design	39	31.5%	-74	9.4%	107	16.5%
Low-noise design	30	-1.5%	-75	10.9%	95	3.1%
Low-noise, improved-bearing-contact design	30	0.0%	-74	10.3%	97	5.7%

Table III. Comparison of static and dynamic stresses, low-noise, improved-bearing-contact design, 100% torque. (n/w = gage not working)

a) Pinion fillet gages 4, 5, 6, 7, 8, 9, 10.

Static Tests

	Gage 4	Gage 5	Gage 6	Gage 7	Gage 8	Gage 9	Gage 10
Max stress (ksi)	87	96	88	85	83	64	40
Min stress (ksi)	-27	-16	-15	-12	-9	-7	-5
Alt stress (ksi)	114	112	102	97	93	71	44

Dynamic Tests

	Gage 4	Gage 5	Gage 6	Gage 7	Gage 8	Gage 9	Gage 10
Max stress (ksi)	82	95	89	n/w	n/w	66	40
Min stress (ksi)	-27	-17	-15	n/w	n/w	-9	-5
Alt stress (ksi)	109	112	105	n/w	n/w	75	46

Difference

	Gage 4	Gage 5	Gage 6	Gage 7	Gage 8	Gage 9	Gage 10
Max stress (ksi)	-6.0%	-1.0%	2.2%	n/w	n/w	2.3%	1.5%
Min stress (ksi)	1.8%	7.9%	2.3%	n/w	n/w	34.7%	16.8%
Alt stress (ksi)	-4.2%	0.3%	2.3%	n/w	n/w	5.4%	3.0%

b) Pinion fillet gages 11, 12, 13, 14, 15, 16, 17.

Static Tests

	Gage 11	Gage 12	Gage 13	Gage 14	Gage 15	Gage 16	Gage 17
Max stress (ksi)	95	90	86	85	77	63	39
Min stress (ksi)	-23	-25	-21	-20	-17	-8	-5
Alt stress (ksi)	119	116	107	105	94	71	44

Dynamic Tests

	Gage 11	Gage 12	Gage 13	Gage 14	Gage 15	Gage 16	Gage 17
Max stress (ksi)	n/w	86	84	85	n/w	67	40
Min stress (ksi)	n/w	-26	-21	-20	n/w	-11	-6
Alt stress (ksi)	n/w	112	105	105	n/w	78	47

Difference

	Gage 11	Gage 12	Gage 13	Gage 14	Gage 15	Gage 16	Gage 17
Max stress (ksi)	n/w	-4.7%	-2.1%	0.0%	n/w	6.4%	3.8%
Min stress (ksi)	n/w	1.6%	-0.6%	-1.9%	n/w	29.1%	33.2%
Alt stress (ksi)	n/w	-3.4%	-1.8%	-0.4%	n/w	9.0%	7.1%

c) Pinion root gages 1, 2, 3.

Static Tests

	Gage 1	Gage 2	Gage 3
Max stress (ksi)	60	59	37
Min stress (ksi)	-49	-42	-17
Alt stress (ksi)	109	101	54

Dynamic Tests

	Gage 1	Gage 2	Gage 3
Max stress (ksi)	n/w	n/w	38
Min stress (ksi)	n/w	n/w	-17
Alt stress (ksi)	n/w	n/w	55

Difference

	Gage 1	Gage 2	Gage 3
Max stress (ksi)	n/w	n/w	3.3%
Min stress (ksi)	n/w	n/w	-3.2%
Alt stress (ksi)	n/w	n/w	1.2%

d) Pinion root gages 18, 19, 20.

Static Tests

	Gage 18	Gage 19	Gage 20
Max stress (ksi)	53	55	41
Min stress (ksi)	-60	-41	-13
Alt stress (ksi)	113	96	55

Dynamic Tests

	Gage 18	Gage 19	Gage 20
Max stress (ksi)	50	54	47
Min stress (ksi)	-65	-43	-15
Alt stress (ksi)	115	97	61

Difference

	Gage 18	Gage 19	Gage 20
Max stress (ksi)	-5.5%	-2.5%	12.5%
Min stress (ksi)	8.2%	6.3%	9.8%
Alt stress (ksi)	1.8%	1.2%	11.8%

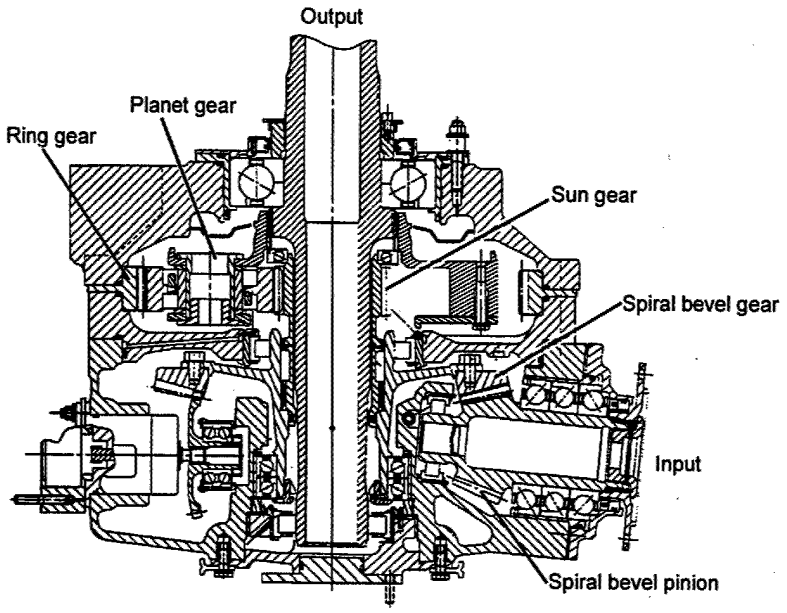

Fig. 1. OH-58D helicopter main-rotor transmission.

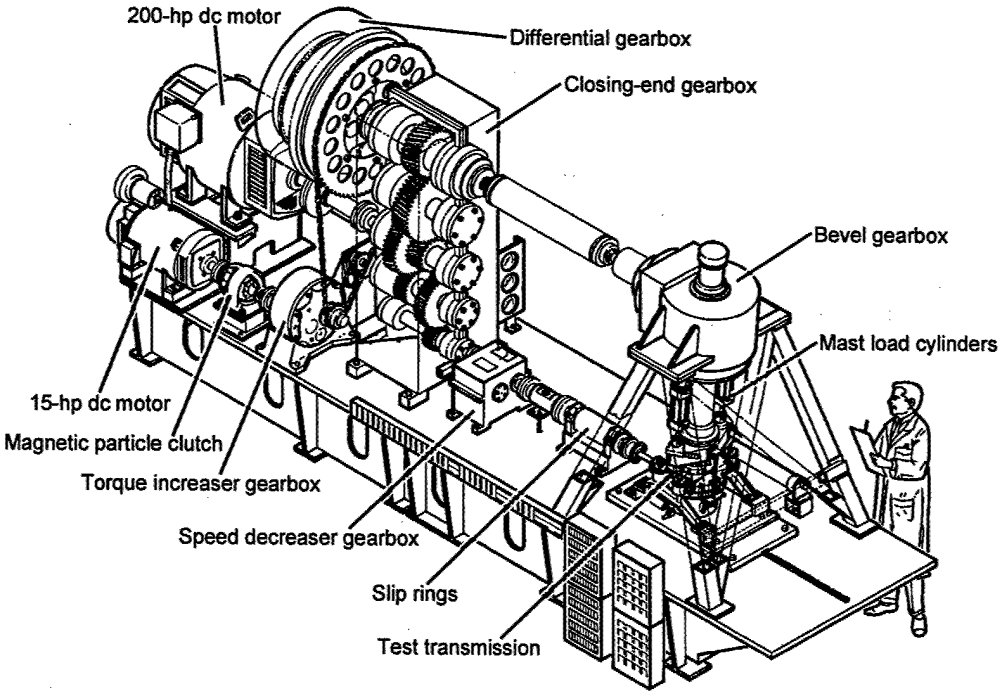

Fig. 2. NASA Glenn 500-hp helicopter transmission test facility.

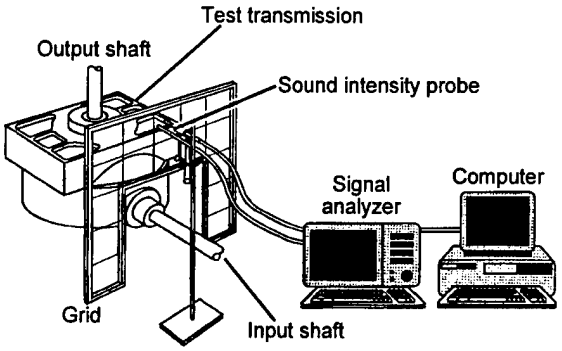

Fig. 3. Sound intensity measurement system.

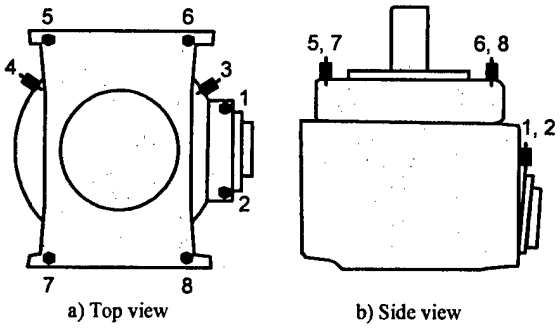

Fig. 4. Accelerometer locations on OH-58D transmission.

Fig. 5. Noise/vibration test setup.

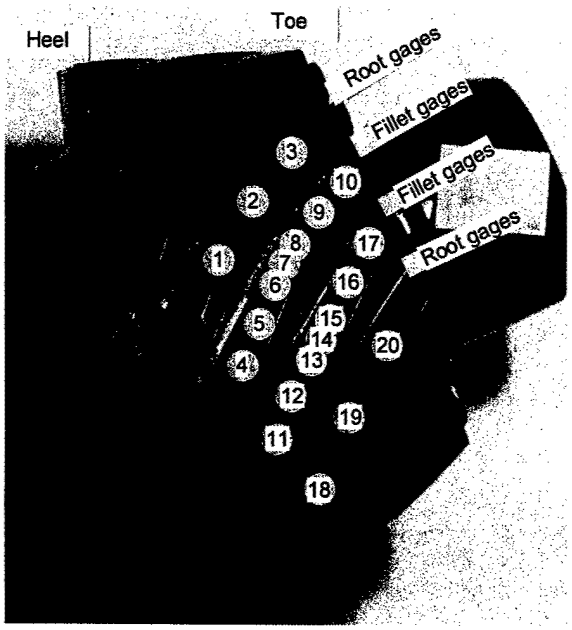

Fig. 6. Strain gage locations on spiral bevel pinion.

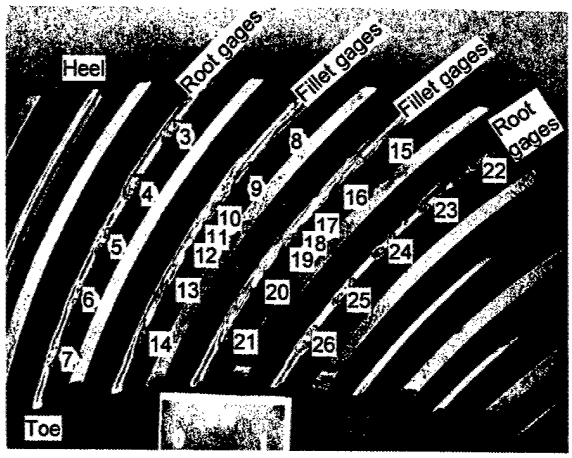

Fig. 7. Strain gage locations on spiral bevel gear.

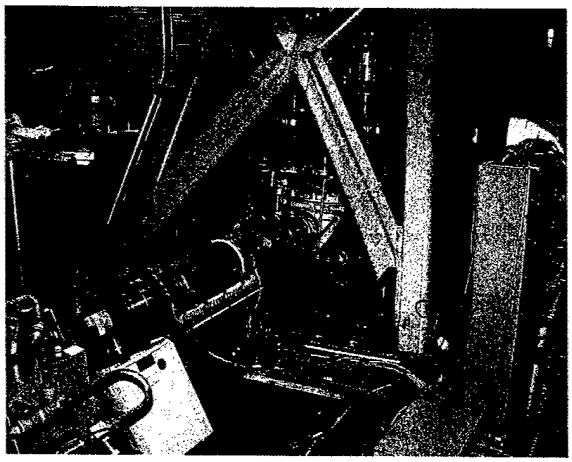

Fig. 8. Static strain test setup.

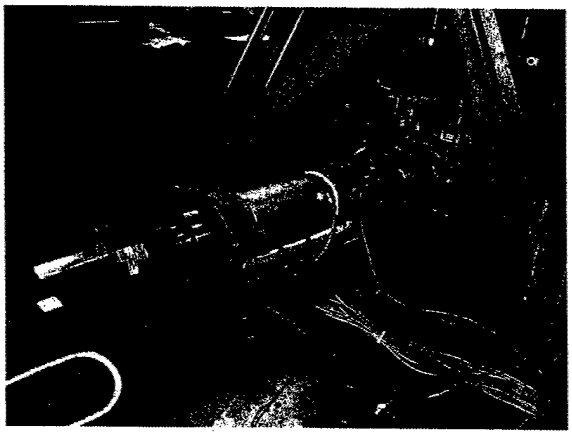

Fig. 9. Dynamic strain test setup..

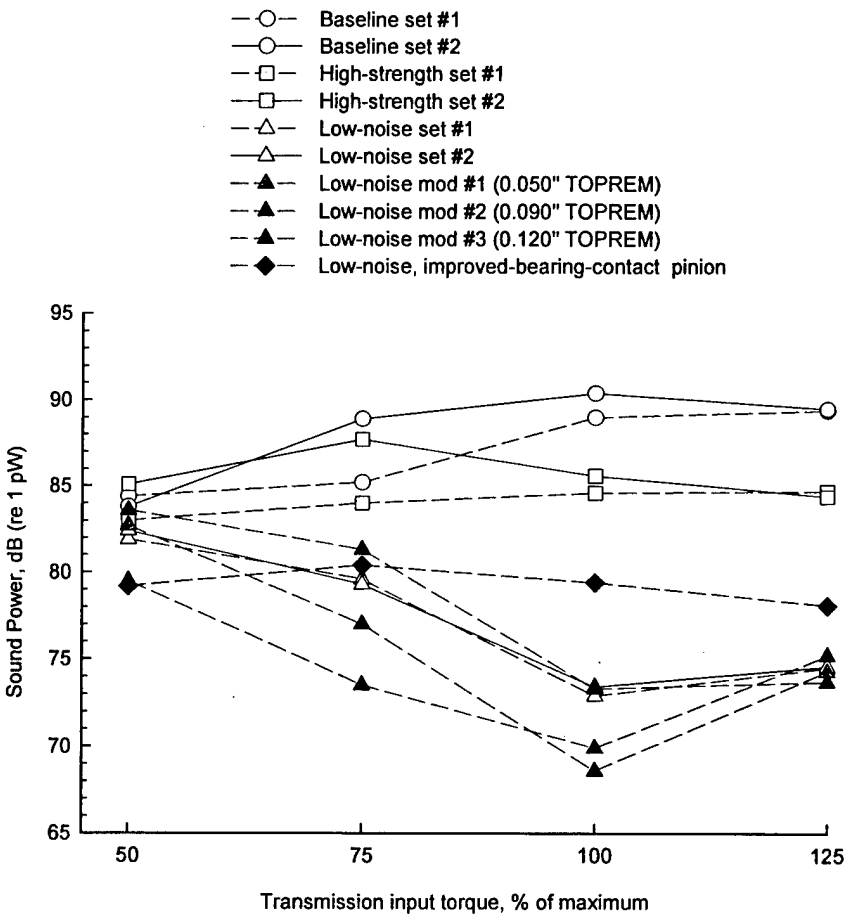

Fig. 10. Sound power at spiral-bevel mesh frequencies.

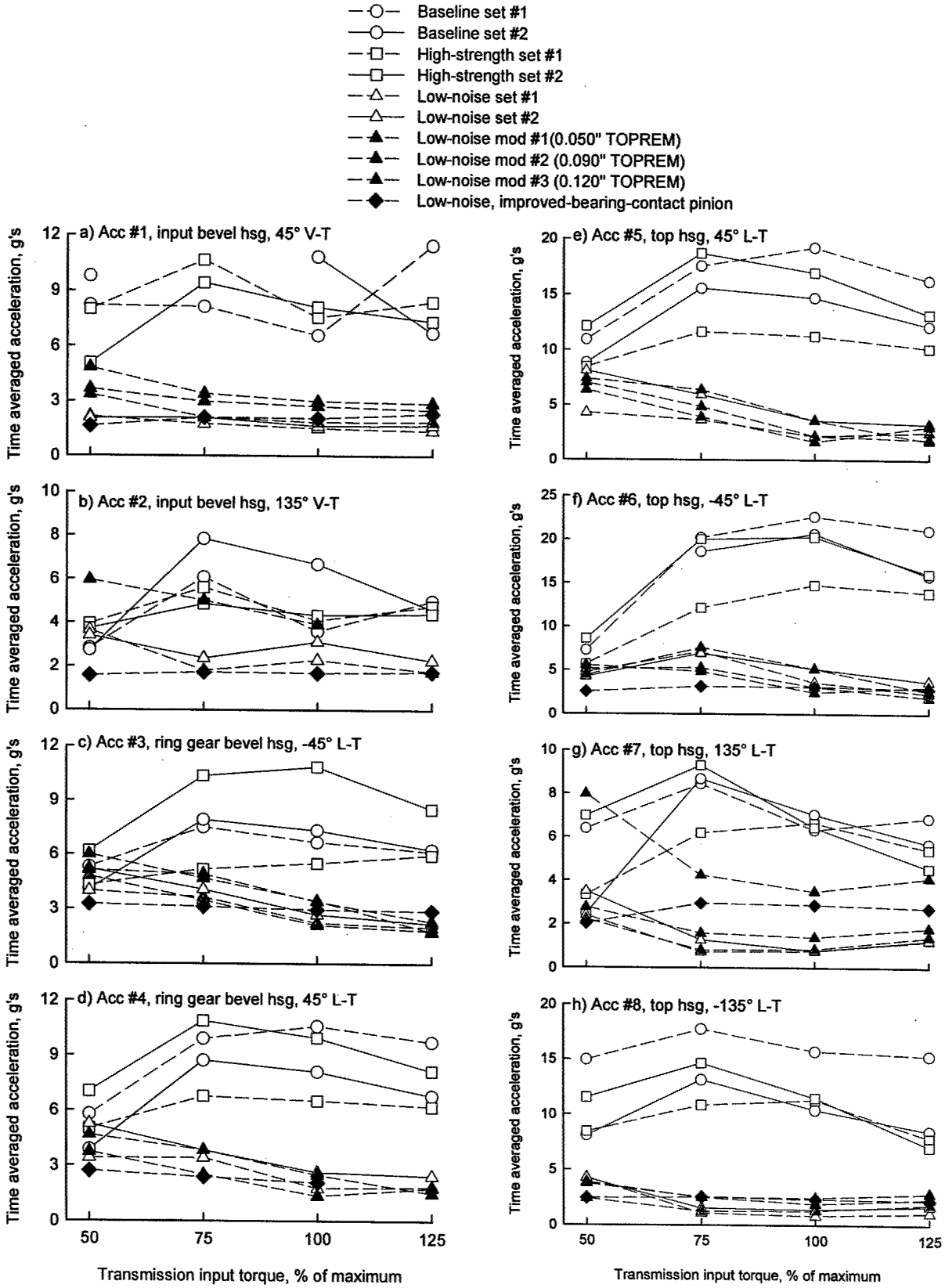

Fig. 11. Vibration results.

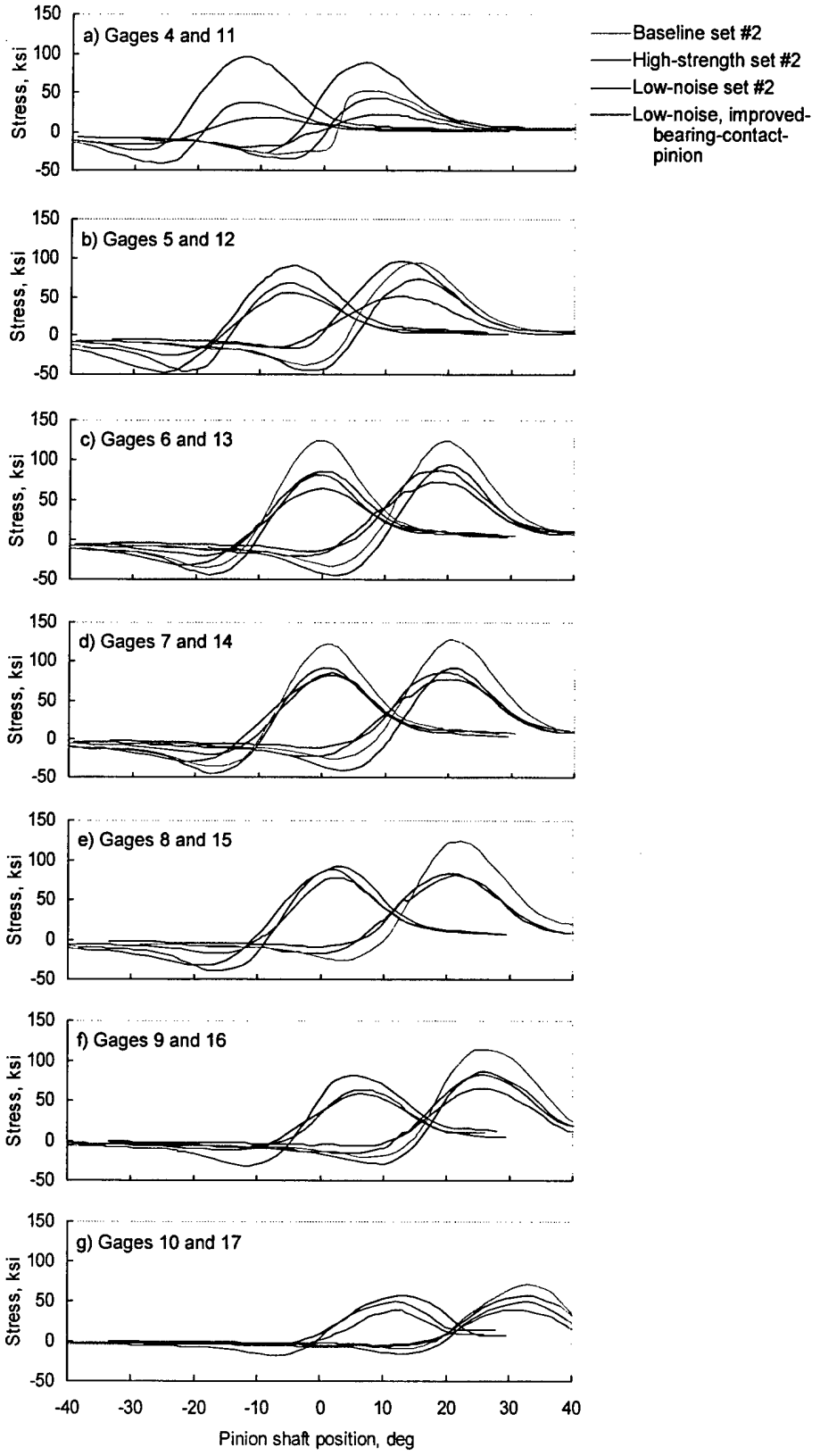

Fig. 12. Results from static strain tests, pinion fillet gages, 100% torque (refer to Fig. 6 for strain gage locations).

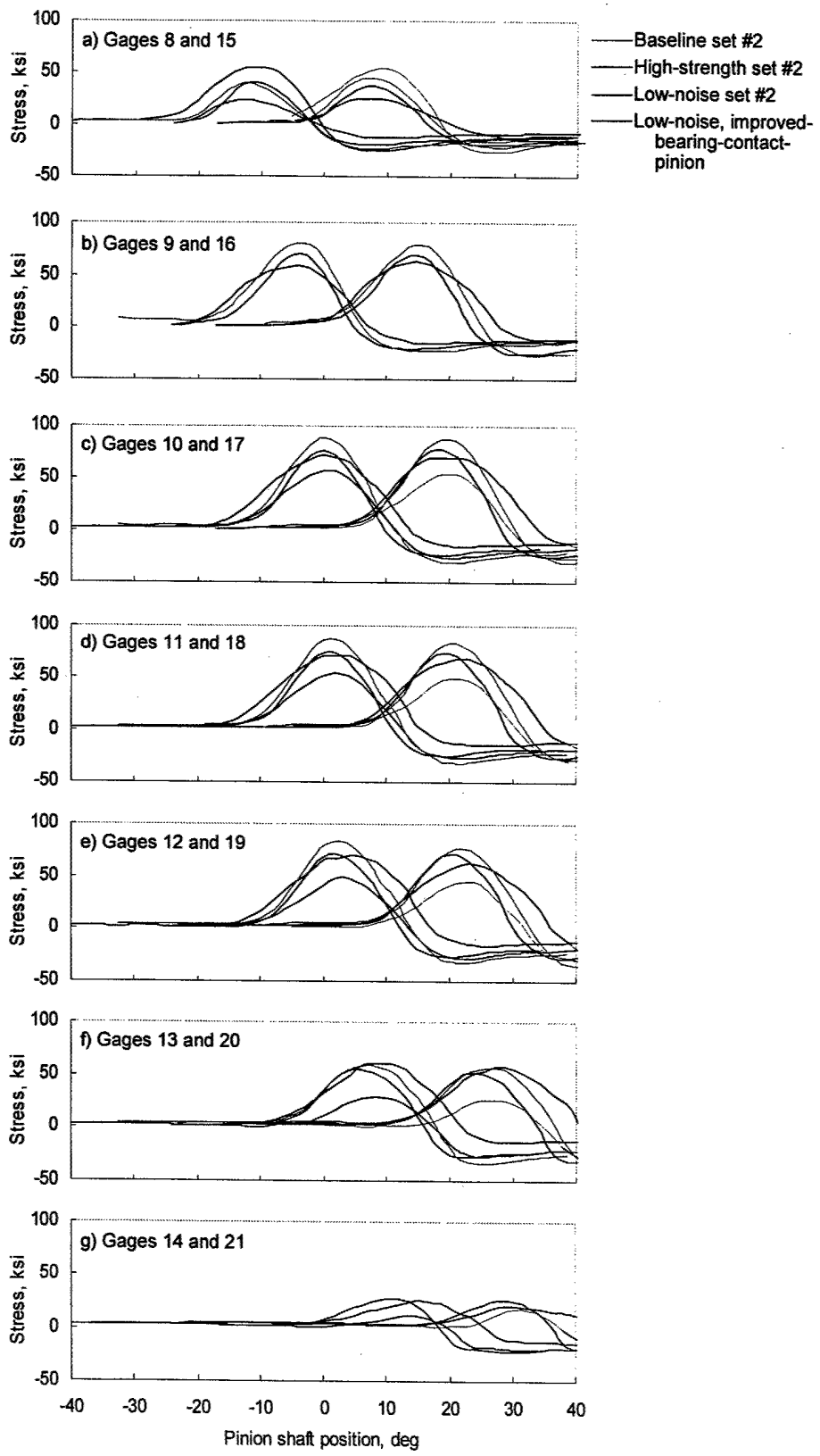

Fig. 13. Results from static strain tests, gear fillet gages, 100% torque (refer to Fig. 7 for strain gage locations).

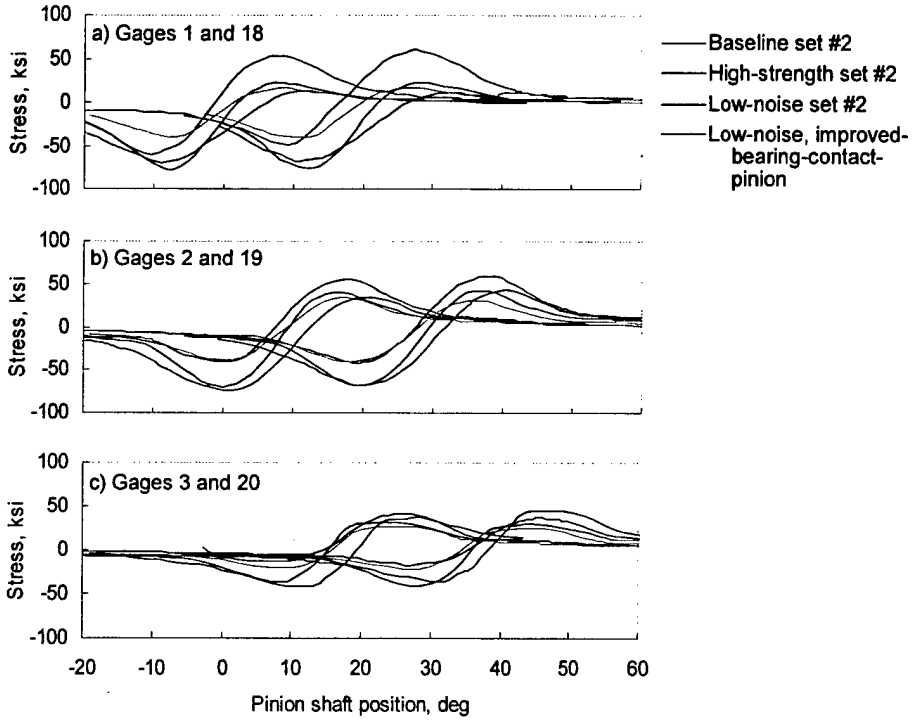

Fig. 14. Results from static strain tests, pinion root gages, 100% torque (refer to Fig. 6 for strain gage locations).

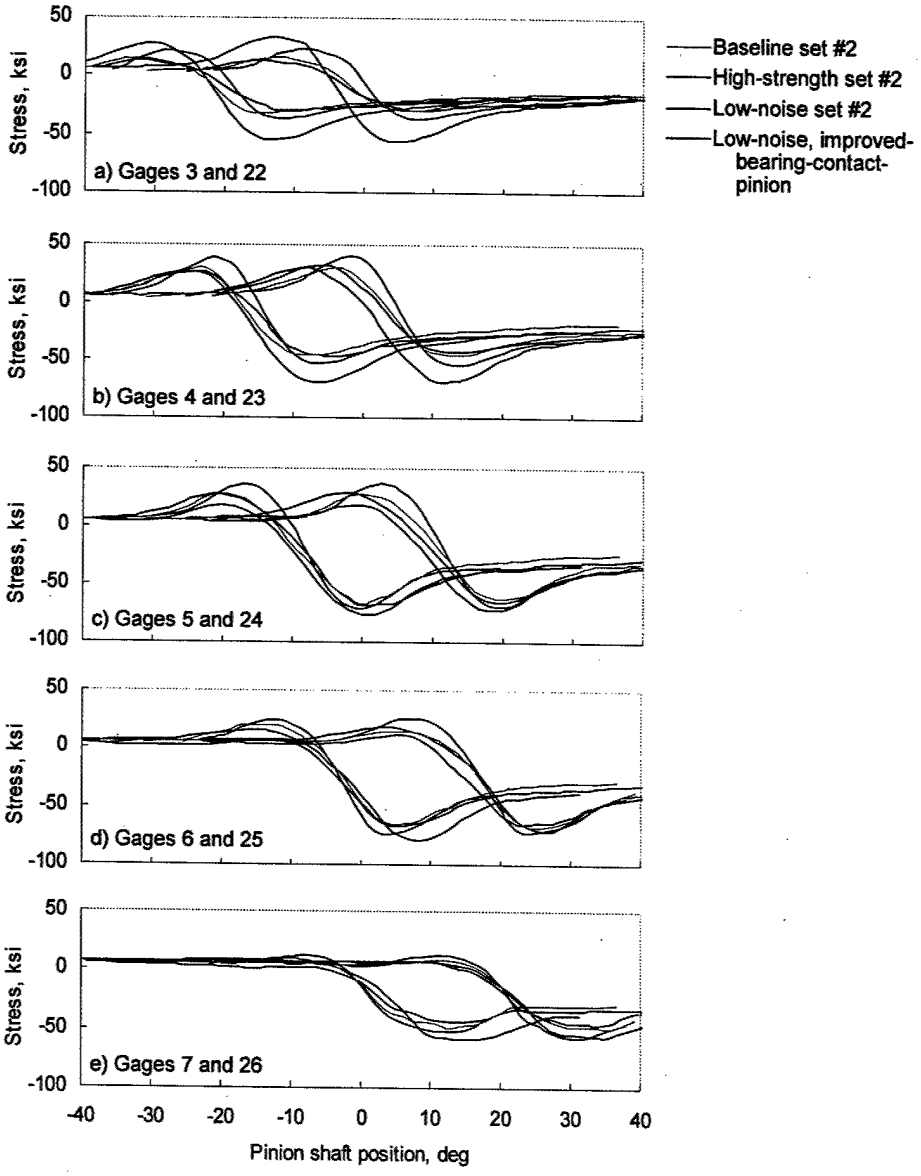

Fig. 15. Results from static strain tests, gear root gages, 100% torque (refer to Fig. 7 for strain gage locations).

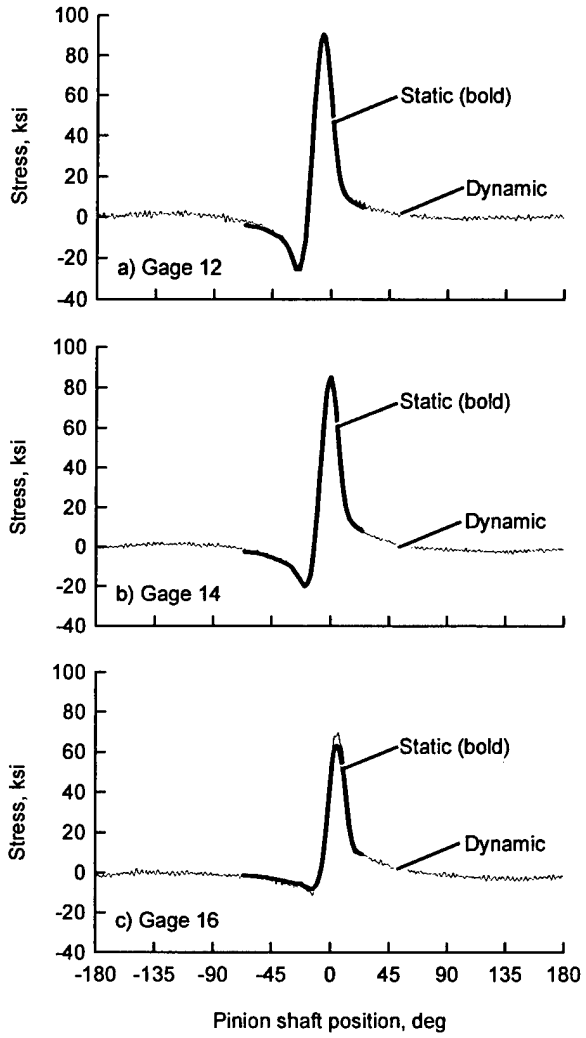

Fig. 16. Comparison of dynamic and static stresses, low-noise, improved-bearing-contact design; pinion fillet gages, 100% torque.

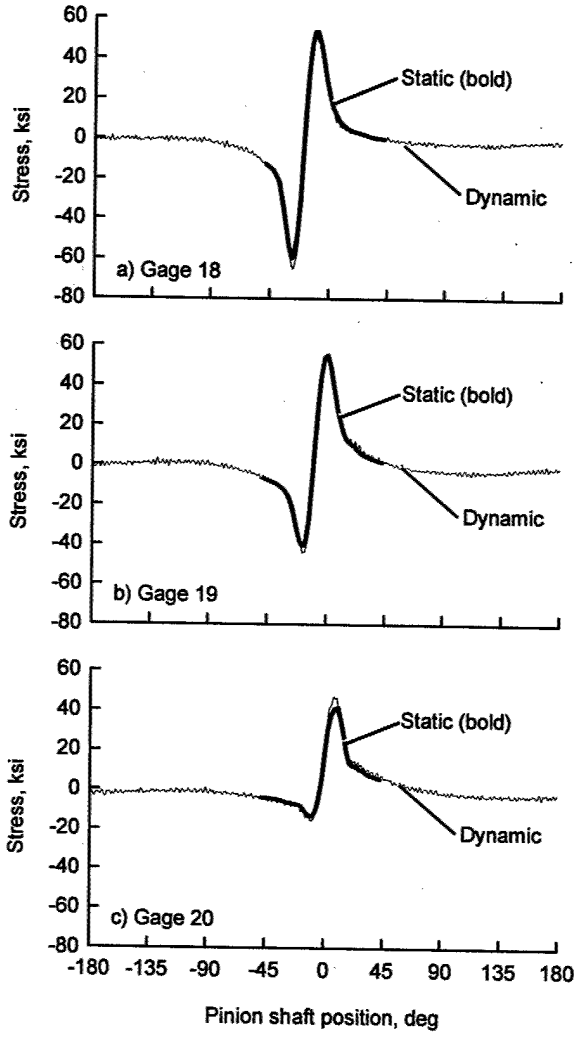

Fig. 17. Comparison of dynamic and static stresses, low-noise, improved-bearing-contact design; pinion root gages, 100% torque.

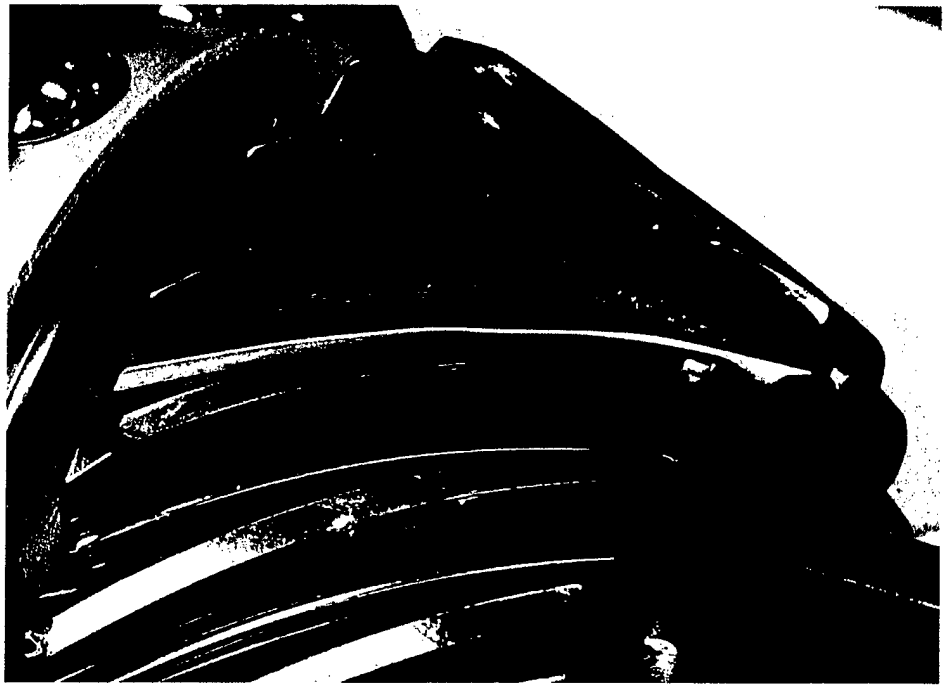

Fig. 18. Spiral-bevel pinion tooth contact, low-noise, improved-bearing-contact design.

Fig. 19. Spiral-bevel gear tooth contact, low-noise, improved-bearing-contact design.